PHYSICAL REVIEW B **68**, 045207 (2003)

Internally consistent approach for modeling solid-state aggregation. II. Mean-field representation of atomistic processes

Manish Prasad and Talid Sinno*
Department of Chemical and Biomolecular Engineering University of Pennsylvania Philadelphia, Pennsylvania 19104-6393

(Received 13 September 2002; revised manuscript received 22 January 2003; published 31 July 2003)

A detailed continuum (mean-field) model is presented that captures quantitatively the evolution of a vacancy cluster size distribution in crystalline silicon simulated directly by large-scale parallel molecular dynamics. The continuum model is parametrized entirely using the results of atomistic simulations based on the same empirical potential used to perform the atomistic aggregation simulation, leading to an internally consistent comparison across the two scales. It is found that an excellent representation of all measured components of the cluster size distribution can be obtained *with consistent parameters* only if the assumed physical mechanisms are captured correctly. In particular, the inclusion of vacancy cluster diffusion and a model to capture the dynamic nature of cluster morphology at high temperature are necessary to reproduce the results of the large-scale atomistic simulation. Dynamic clusters with large capture volumes at high temperature, which are the result of rapid cluster shape fluctuations, are shown to be larger than would be expected from static analyses, leading to substantial enhancement of the nucleation rate. Based on these results, it is shown that a parametrically consistent atomistic-continuum comparison can be used as a sensitive framework for formulating accurate continuum models of complex phenomena such as defect aggregation in solids.

DOI: 10.1103/PhysRevB.68.045207 PACS number(s): 61.72.Ji

I. INTRODUCTION

An important challenge in the formulation of continuum rate equation-based models for inherently atomistic processes is verification of the physics and chemistry embodied within the model.[1–6] Typically in such models, both the assumed mechanisms and the model parameters are uncertain. The latter are often fitted to experimental data but are reliable only if the model used to perform the data regression is mechanistically accurate.[7–9] As a result, an increase in the number of fitting parameters usually is associated with an increase in the uncertainty of the assumed physical and chemical mechanisms.

An alternative approach to model parameterization with experimental data is to use atomistic simulation to compute independently the required thermophysical property information.[10–14] However, in the case of microstructural evolution in crystalline semiconductors, it has been shown that even the state-of-the-art *ab initio* methods[15–18] are not yet able to compute sufficiently accurately properties such as intrinsic point defect diffusivities and equilibrium concentrations for use in continuum process models.[19] Other approaches such as the kinetic Monte Carlo method[20,21] also require a substantial physical property and mechanistic description input; see Ref. 22 for a brief review of previous studies based on these approaches.

The goal of the work described here and in Ref. 22 (hereafter referred to as Paper I) is to use atomistic simulation to characterize the important mechanistic processes, rather than thermophysical properties during vacancy aggregation in crystalline silicon. The central element is a parametrically consistent comparison between two representations (atomistic and continuum) of a single process in order to develop a mechanistically accurate continuum model as discussed in Paper I. Parametric consistency is ensured by requiring that all thermophysical property information needed for the continuum model is generated by atomistic simulations employing the same interatomic potential used to directly model the process atomistically. In the present work, the focus is on the aggregation of vacancies in crystalline silicon. The quantitative understanding of void (large octahedral vacancy clusters) (Ref. 23) formation during silicon crystal growth and wafer processing remains technologically important, and the detrimental effects of voids on the performance of DRAM memory devices are well documented.[24] Finally, a plethora of quantitative experimental data is available for model parameterization and testing.

A comprehensive atomistic analysis was presented in Paper I that led to compact representations of vacancy cluster thermodynamics and transport, particularly equilibrium cluster structures, free energies and diffusion coefficients as a function of temperature. The environment dependent interatomic potential[25,26] (EDIP) was used for all simulations. A single large-scale molecular dynamics simulation was then performed in which 1000 vacancies were placed in a silicon host lattice containing 216 000 sites. The system was allowed to evolve in the NVT ensemble at 1600 K and zero pressure and the size distribution of vacancy clusters monitored as a function of time. It was found that essential features, namely the evolution in time of the average cluster size, of the vacancy aggregation profile could be captured with a simple mean-field scaling analysis.[27,28] However, certain unjustified approximations, such as irreversible, homogeneous aggregation rates, were necessary to generate the analytic mean-field result, and the goal of the current paper is to remove these in order to formulate a predictive process model.

In this paper, a detailed continuum model suitable for use in process scale simulation of crystal growth and wafer processing is developed and investigated by comparing the predicted cluster size evolution to the results of the atomistic simulation. The paper is structured as follows. The overall description of the model is presented in Sec. II, where the rate equations and the thermodynamics associated with cluster formation and dissolution are discussed in detail. In Sec. III, kinetic models for these processes are developed based on extensions of previous work. In Sec. IV, molecular statics simulations are presented, which are aimed at computing quantitative estimates for the interaction distances between clusters as a function of cluster size. These predictions are then used to compute mean-field estimates for the cluster size distribution and are compared to the atomistic simulation results. In Sec. V, a cluster capture radius model that accounts for the effect of high temperature on cluster morphology, mobility and mutual interaction is developed based on the results of further atomic simulations and this model is used to refine the continuum representation. A sensitivity analysis is presented in Sec. VI, which demonstrates the contribution of each part of the overall continuum model as well as the robustness of the overall approach. Finally, conclusions are presented in Sec. VII.

II. CONTINUUM MODEL OF VACANCY AGGREGATION

In this section, a general theoretical framework for continuum modeling of vacancy aggregation based on coupled rate equations is developed. Such models are necessary for extending the scope of atomistic simulations to realistic processing environments such as crystal growth and wafer annealing.[1,2,3,29] The model is first developed using a single reaction pathway in which only monomers are assumed to be mobile and then is extended to the general case of cluster diffusion and reaction. The continuum model described here is based on a system of coupled Master equations due to Smoluchowski:[30]

$$\frac{dX_k}{dt} = \frac{1}{2}\sum_{i+j=k}[K(i,j)X_iX_j - F(i,j)X_{i+j}] - \sum_{j=1}^{\infty}[K(k,j)X_kX_j - F(k,j)X_{k+j}], \tag{2.1}$$

where X_k is the number of clusters of size k, $K(i,j)$ is the coagulation kernel (i.e. the set of forward reaction rates) between two clusters of size i and j, respectively, and $F(i,j)$ is the fragmentation kernel, which describes the rate of dissociation of a cluster of size $i+j$ into clusters of size i and j.

A. General thermodynamic considerations

The bimolecular reaction $V_i + V_1 \underset{F(i,1)}{\overset{K(i,1)}{\leftrightarrow}} V_{i+1}$ proceeds at the *net* forward flux, J_i, which is given by[3,31,32]

$$J_i = K(i,1)X_iX_1\exp\left(-\frac{\Delta G^B_{i+1\to(i+1)}}{kT}\right) - F(i,1)X_{i+1} \times \exp\left(-\frac{\Delta G^B_{(i+1)\to i+1}}{kT}\right), \tag{2.2}$$

where $\Delta G^B_{i+1\to(i+1)}$ is the free energy barrier for the growth of a cluster of size i into one of size $i+1$ by the incorporation of a monomer. The rate, or master,[3,33] equation for the temporal evolution of species i can be written as

$$\frac{dX_i}{dt} = J_{i-1} - J_i, \quad 2 \leqslant i \leqslant N_{\max} - 1, \tag{2.3}$$

where $N_{\max}$ is the largest cluster considered in the continuum model. The rate equations appropriate at the size-space boundaries, $N=1$ and $N=N_{\max}$, respectively, are given by

$$\frac{dX_1}{dt} = -J_1 - \sum_{i=1}^{i=N_{\max}-1} J_i, \tag{2.4}$$

and

$$\frac{dX_{N_{\max}}}{dt} = J_{N_{\max}-1}. \tag{2.5}$$

Equation (2.5) represents a no-flux boundary condition at the largest cluster size, and does not affect the resulting size distribution if $N_{\max}$ is chosen to be sufficiently large.

The free energy of a system containing vacancies and vacancy clusters is written as[34]

$$G^{System} = G^0 + \sum_i X_i G_i^f - kT\cdot\ln\Omega, \tag{2.6}$$

where G_i^f is the vibrational free energy of formation of clusters of size i,k the Boltzmann constant, T the temperature of the system and

$$\Omega = \prod_i \frac{(i)^{X_i}\cdot(N/i)!}{(N/i - X_i)!(X_i)!} \tag{2.7}$$

is the total number of possible ways of distributing $\{X_i\}$ clusters in a lattice containing N sites.[35] The $-kT\ln(\Omega)$ term represents the configurational entropy. The total free energy barrier associated with the forward component $K(i,1)$ in Eq. (2.2) is then given by[32]

$$\Delta G^B_{i+1\to(i+1)} = G^f_{i+1} - G^f_i - G^f_1 - kT\cdot\ln\left(\frac{\Omega_2}{\Omega_1}\right) + \Delta E^B, \tag{2.8a}$$

$$\frac{\Omega_2}{\Omega_1} = \frac{(i+1)\cdot\left(\frac{N}{(i+1)} - X_{(i+1)}\right)\cdot X_i\cdot X_1}{i\cdot\left(\frac{N}{i} - X_i + 1\right)\cdot(N - X_1 + 1)\cdot(X_{(i+1)}+1)} \tag{2.8b}$$

if $G^f_{i+1} - G^f_i - G^f_1 - kT\cdot\ln(\Omega_2/\Omega_1) \geqslant 0$, i.e., the free energy of the system is higher after the aggregation step, $i+1\to(i+1)$, has taken place. The subscripts, 1 and 2, on the Ω terms represent the initial state $\{X_1,\ldots,X_i,X_{i+1},\ldots\}$ and the final state $\{X_1-1,\ldots,X_i-1,X_{i+1}+1,\ldots\}$ of the reaction, respectively. The total free energy barrier is simply

$$\Delta G^B_{i+1\to(i+1)} = \Delta E^B, \tag{2.9}$$

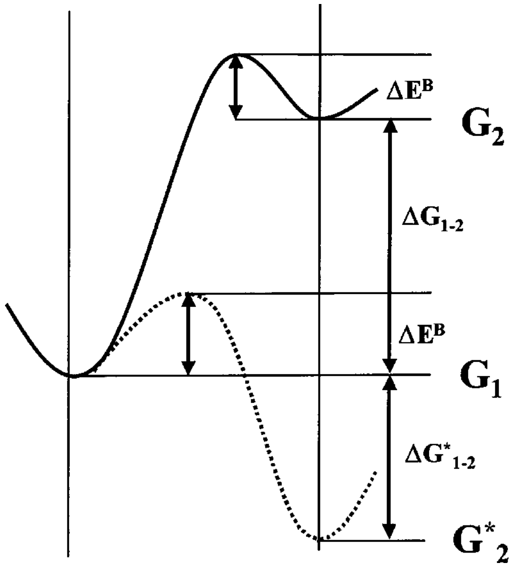

FIG. 1. Total system free energy as a function of reaction coordinate during an aggregation event: (a) Total free energy increases (G_1-G_2) following aggregation. (b) Total free energy decreases $(G_1-G_2^*)$ following aggregation.

if $G_{i+1}^f-G_i^f-G_1^f-kT\cdot\ln(\Omega_2/\Omega_1)<0$, implying that the total free energy has been reduced following the aggregation step. Here ΔE^B is an enthalpic barrier that may or may not be present, depending on any structural rearrangements that need to be made during the incorporation of the monomer. The two cases represented by Eqs. (2.8) and (2.9) are shown schematically in Fig. 1. Similar arguments can be made for the reverse reaction, in which a monomer is emitted and a cluster of size $i+1$ shrinks to a cluster of size i. In other words, if the net free energy change following any reaction is negative, the barrier is ΔE^B and the free energy difference does not affect the reaction rate.

At equilibrium, the rate of change in the concentration of each cluster size is zero as is the free energy change associated with any cluster growth or dissolution process, and therefore, for all i, the forward and backward reaction rates are equal:[34]

$$\frac{\text{Forward Rate}}{\text{Backward Rate}}=\frac{K(i,1)\cdot X_i^{\mathrm{eq}}\cdot X_1^{\mathrm{eq}}}{F(i,1)\cdot X_{i+1}^{\mathrm{eq}}}\times\exp\left(-\frac{\Delta G_{i+1\to(i+1)}^{\mathrm{eq}}}{kT}\right)=1, \tag{2.10}$$

where X_i^{eq} is the equilibrium number of clusters of size i and

$$\Delta G_{i+1\to(i+1)}^{\mathrm{eq}}=G_{i+1}^f-G_i^f-G_1^f-kT\cdot\ln\left(\frac{\Omega_2^{\mathrm{eq}}}{\Omega_1^{\mathrm{eq}}}\right)=0. \tag{2.11}$$

Note that Eqs. (2.10) and (2.11) are thermodynamic requirements for equilibrium and always are valid irrespective of the reaction under consideration. Equation (2.10) also determines the backward reaction rate in terms of the forward one and the equilibrium concentrations of the relevant species,[34] so that

$$F(i,1)=\frac{K(i,1)\cdot X_i^{\mathrm{eq}}\cdot X_1^{\mathrm{eq}}}{X_{i+1}^{\mathrm{eq}}}. \tag{2.12}$$

The large-scale atomistic simulation system described in Paper I is a thermodynamically closed system in which the total number of vacancies and Si atoms are conserved. Thus, a mean-field model must be based on consistent thermodynamics. Therefore, the equilibrium distribution of vacancy clusters $\{X_i^{\mathrm{eq}}\}$ in Eq. (2.12) should correspond to the constrained equilibrium conditions in a closed system with a fixed number of vacancies, and not the unconstrained (open system) equilibrium distribution. In the remainder of this paper, it is implied that all equilibrium concentrations are computed self-consistently by minimizing the total free energy of the closed system; see Paper I for details. It also is worthwhile noting here that the actual values of the equilibrium concentrations are expected to be important only for longer times, and are found not to affect the cluster size distribution significantly over $O(10^{-9}-10^{-8})$ seconds.

B. Cluster diffusion

The inclusion of cluster diffusion into the continuum model represented by Eqs. (2.2)–(2.12) requires that additional reaction pathways for cluster growth (and dissolution) be considered. Extending the above reaction framework to include cluster diffusion is straightforward. Almost all of the above equations [i.e., Eqs. (2.2)–(2.12)] can be modified to include j-mer diffusion simply by replacing the index "1" by "j." The reaction pathway for cluster growth by cluster-cluster reaction is now given by

$$V_i+V_j\underset{F(i,j)}{\overset{K(i,j)}{\leftrightarrow}}V_{i+j}. \tag{2.13}$$

The *net* forward flux for this reaction is[36,37]

$$J_i^j=K(i,j)\cdot X_i\cdot X_j\cdot\exp\left(-\frac{\Delta G_{i+j\to(i+j)}^B}{kT}\right)-F(i,j)\times X_{i+j}\cdot\exp\left(-\frac{\Delta G_{(i+j)\to i+j}^B}{kT}\right), \tag{2.14}$$

where $\Delta G_{i+j\to(i+j)}^B$ is the total free energy barrier associated with the coalescence of a cluster of size i and a cluster of size j. Equation (2.7) remains the same as before, but the configurational free energy change due to the coalescence of two clusters is now given by

$$\frac{\Omega_2}{\Omega_1}=\frac{(i+j)\cdot\left(\dfrac{N}{(i+j)}-X_{(i+j)}\right)\cdot X_i\cdot X_j}{i\cdot j\cdot\left(\dfrac{N}{i}-X_i+1\right)\cdot\left(\dfrac{N}{j}-X_j+1\right)\cdot(X_{(i+j)}+1)}. \tag{2.15}$$

The appropriate coupled rate equations are now given by the following system of equations:

$$\frac{dX_i}{dt}=\sum_{j=1}^{i-1}\left[J_{i-j}^{j}-J_{i}^{j}\right]-J_i^i-\sum_{j\geqslant i}^{N_{\max}-i}J_j^i,\quad 1\leqslant i\leqslant N_d, \tag{2.16a}$$

$$\frac{dX_i}{dt}=\sum_{j=1}^{N_d}\left[J_{i-j}^{j}-J_{i}^{j}\right],\quad N_d<i\leqslant N_{\max}-1, \tag{2.16b}$$

$$\frac{dX_i}{dt}=\sum_{j=1}^{N_d}\left[J_{i-j}^{j}\right],\quad i=N_{\max}, \tag{2.16c}$$

$$J_i^j=0,\quad j>i. \tag{2.16d}$$

In Eqs. (2.16), N_d is the number of diffusing clusters, and J_i^j is defined as the net forward flux at size *i* due to the reaction enabled by a diffusor of size *j*. The results of Sec. IV in Paper I demonstrated that cluster diffusion rates decay as $j^{-1.25}$, and therefore all clusters are, in principle, mobile. However, because of the finite size and small time of the atomistic simulation and therefore few large clusters, N_d is taken to be ten as determined by sensitivity analysis.

III. REACTION MODELING

The final component needed to specify completely the continuum model for vacancy aggregation is a set of forward reaction rate constants, $K(i,j)$, noting once again that the fragmentation rates, $F(i,j)$, can be computed from these if the constrained equilibrium concentrations are known. The overall coalescence rate between two clusters is determined by two series mass transfer resistances: diffusion within the lattice until the two species are within a capture distance, $r_{\text{cap}}(i,j)$ of each other, followed by reaction at the cluster surfaces. The capture distance is defined as the point-to-point distance between the clusters' centers of mass at which the interaction energy is non-zero. We use a model that was previously developed to describe the attachment of a single vacancy to a cluster,[3,31] which is readily generalized to include reaction between two diffusing clusters.

Lifshitz and Slyozov[38] have treated the kinetics of this problem by considering a reference stationary reactant, *i*, which is surrounded by a distribution of *j*'s. The diffusive flux of *j* species at the interaction distance, $r_{\text{cap}}(i,j)$, of the reference particle *i* is matched by the incorporation rate of *j*'s into *i*, so that[3]

$$\frac{4\pi r_{\text{cap}}^2(D_i+D_j)}{V}\left[\frac{\partial X_j}{\partial r}\right]_{\text{rcap}}=K(i,j)\exp\left(-\frac{\Delta G^B_{i+j\to(i+j)}}{kT}\right)\times[X_j(r_{\text{cap}})-X_j^{\text{eq}}(r_{\text{cap}})]. \tag{3.1}$$

The number of clusters of species *j* and its spatial gradient at $r_{\text{cap}}(i,j)$ is obtained via the steady state solution of the spherically symmetric diffusion equation about the reference particle *i*. The equilibrium number of clusters of species *j* at $r_{\text{cap}}(i,j)$, $X_j^{\text{eq}}(r_{\text{cap}})$, is taken to be equal to its bulk value X_j^{eq}. Using this result and rearranging Eq. (3.1), the concentration of *j* at the surface of the reference *i* particle is given by

$$X_j(r_{\text{cap}},i)=\frac{K(i,j)\exp(-\Delta G^B_{i+j\to(i+j)}/kT)X_j^{\text{eq}}(r_{\text{cap}})+k^d_{i+j}X_j(\text{bulk})}{K(i,j)\exp(-\Delta G^B_{i+j\to(i+j)}/kT)+k^d_{i+j}}, \tag{3.2}$$

where

$$k^d_{i+j}=\frac{4\pi r_{\text{cap}}(i,j)}{V}(D_i+D_j)$$

(Refs. 30, 39, and 40). The expression for k^d_{i+j} differs from previous expressions for diffusion limited reaction rate given in Refs. 30, 39, and 40 by a factor of V^{-1}, where V is the system volume (see Sec. IV B), because of use of cluster numbers rather than concentrations as our basis for formulating Eqs. (2.2)–(2.5) and (2.16). Equation (3.2) is generally valid in the sense that it does not assume that the aggregation process is either diffusion or reaction limited. An expression for $K(i,j)$ is derived by using jump rate theory[41] and assuming that the final step for cluster-cluster reaction corresponds to a single vacancy jump over a distance δ, which is taken here to correspond to the lattice parameter, i.e., $\delta=0.235$ nm. The jump rate is given by[41] $\nu_{i,j}=\nu^0_{i,j}\exp(-E^d_{i,j}/kT)$, where $E^d_{i,j}$ is the energy barrier for diffusion across the interface between clusters *i* and *j*.

The volume over a thickness of δ, surrounding the reference cluster, *i*, is given by $\delta\cdot 4\pi R_i^2$, and therefore the number of *j*-clusters that can attempt to attach to *i* is $\delta\cdot 4\pi R_i^2 C_j(r_{\text{cap}}(i,j))$, where $C_j=X_j/V$. The forward reaction rate for $i+j\to(i+j)$ is therefore given by[33]

$$K(i,j)=\frac{4\nu_{i,j}\delta\pi R_i^2}{V}. \tag{3.3}$$

In general, both $\nu_{i,j}$ and $E^d_{i,j}$ may vary with *i* and *j*, particularly for small clusters. However, these effects are expected to be quite small and difficult to quantify, hence both quantities are assumed to be constant, i.e. $\nu_{i,j}=\nu$ and $E^d_{i,j}=E^d$.[41,42] Equation (3.3) can be combined with the general jump rate theory expression for diffusion,[41]

$$D_d=\delta^2\nu_d\exp(-E_d/kT), \tag{3.4}$$

to give[3,31,32,33]

$$K(i,j)=\frac{4\pi D_j r_{\mathrm{cap}}^2(i,j)}{V\delta}. \tag{3.5}$$

For the general case of agglomeration of two diffusing clusters, Eq. (3.5) is written as

$$K(i,j)=\frac{4\pi}{V\delta}(D_i+D_j)r_{\mathrm{cap}}^2(i,j). \tag{3.6}$$

Now, all the essential ingredients, except $r_{\mathrm{cap}}(i,j)$ for a general continuum model have been specified. In principle, once all the required thermophysical properties are computed, a quantitatively accurate representation of the atomic scale evolution profile should be obtained if the model is a good representation of the atomic process. The remainder of this paper compares the predictions of the continuum model described in the previous three sections with the atomistic results shown in figure 14 in Paper I.

IV. COMPACT CLUSTER MODEL

In this section, it is assumed that the structures and free energies of the actual vacancy clusters observed during the atomistic simulation are well described by the hexagonal-ring cluster (HRC) model.[43,44] Given this assumption, only the cluster capture radii need to be computed before a numerical solution of the model described above can be obtained. The effective capture radius around an individual cluster depends on several factors, such as the cluster size, morphology, and resulting strain on the surrounding lattice. The total capture radius is defined here as the sum of the characteristic radius of the actual cluster and the distance at which sufficient lattice distortion occurs to make the cluster's presence ''felt'' by another entity.

A. Vacancy-Vacancy Interactions

The capture distance between vacancy clusters first was investigated by considering two single vacancies. The results in Paper I indicate that the vacancy dimer binding energy approaches zero at the fourth; nearest neighbor distance measured along the (110) direction (4NN-110). These results are fully consistent with the Stillinger-Weber results of Bongiorno *et al.*,[45] who found that two vacancies with initial separation less than or equal to 4NN-110 bind immediately in low-temperature molecular dynamics simulations, while those at more than 4NN-110 separation will diffuse randomly. The vacancy-vacancy capture radius based on these analyses therefore can be taken as 7.67 Å, which corresponds to the 4NN-110 distance in the perfect crystal at zero pressure. This conclusion also is in good agreement with previous estimates based on the analysis of positron annihilation data.[46] Note that the capture distance is lower than this value when the two vacancies are connected along a non-(110) direction, but it is assumed here that the largest capture distance determines the overall kinetics.

Static relaxations of various vacancy-vacancy configurations were performed using the EDIP potential. Based on these calculations, details of which will be provided elsewhere, a critical atomic displacement is estimated at about 0.07 Å. This value represents the local atomic displacement required for a vacancy (or vacancy cluster) to ''detect'' the presence of another vacancy entity leading to binding if the thermodynamics are favorable.

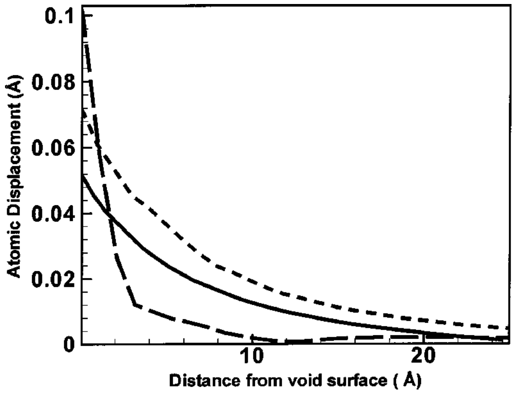

FIG. 2. Spatial propagation of the displacement field along (a) (100) (solid line); (b) (110) (dashed line), and (c) (111) (long-dashed lines).

B. Cluster-Cluster Interactions

The dependence of the cluster capture radius on cluster size was investigated using static relaxations of systems containing octahedral voids of different sizes.[44] Two void sizes were considered in these calculations—165 and 455 vacancies—both sizes correspond to ''perfect clusters'' with regular octahedral geometry. The spatial evolution of the displacement field from the cluster surface in several directions is shown in Fig. 2. Shown are the atomic displacements along the (100), (110), and (111) directions, which correspond to normal vectors to the cluster base corner, base edge, and pyramidal plane, respectively. The displacement is largest normal to the (111) plane, indicating a contraction of the lattice into the void. Conversely, the displacement field is smallest along the (100) direction. Also notable is the fact that the displacement field goes down most rapidly along the (111) direction while the decay along (100) is slowest. Nevertheless, displacements along all three directions are observed to decay rapidly below the critical 0.07-Å value at a distance of about 3–4 Å from the cluster surface. Similar results are found for the smaller 165-vacancy cluster as expected. These findings are entirely consistent with the observation that octahedral vacancy clusters found in commercial CZ silicon appear to induce a negligible strain field when observed by TEM.[47,48]

The total capture radius for a cluster containing j vacancies therefore can be expressed as

$$R_j^{\mathrm{tot}}=R_j+r_{\mathrm{str}}, \tag{4.1}$$

where $r_{\mathrm{str}}=3.84$ Å, which is one-half of the 4NN-110 distance, represents the lattice strain field contribution to the capture radius and is a constant for all cluster sizes, and R_j is the contribution based on the actual cluster size. Note that the capture distance for two clusters, i and j, is then given by $R_i^{\mathrm{tot}}+R_j^{\mathrm{tot}}\equiv r_{\mathrm{cap}}(i,j)$. Total capture radii for HRC clusters were computed as follows. For each vacancy in each HRC

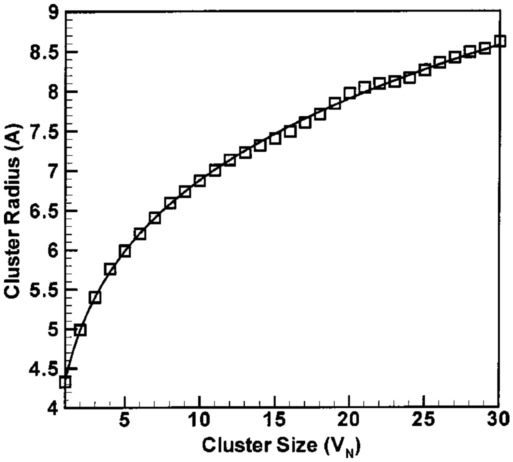

FIG. 3. Evolution of total radius, $R_j^{\mathrm{tot}}(j)$, as a function of cluster size for HRC clusters. The total radius includes 50% of the vacancy-vacancy interaction distance due to lattice distortion. The solid line is a power-law fit.

cluster, all atoms within a 2NN distance were recorded. The resulting object represents both the cluster and its capture zone. We assume here that these volumes are approximately spherical and therefore $R_j^{\mathrm{tot}}=(3V_j^{\mathrm{tot}}/4\pi)^{1/3}$, where V_j^{tot} is defined as total cluster capture volume, i.e., the volume of the cluster containing j vacancies and its associated capture zone. A plot of $R_j^{\mathrm{tot}}(j)$ as a power-law function of cluster size is shown in Fig. 3 (compact cluster model), along with the sizes predicted by other models. Large cluster capture volumes can greatly reduce the free volume in a finite system. Excluded volume was computed as $V^{\mathrm{ex}}=\sum_{j=1}^{N_{\max}}X_jV_j^{\mathrm{tot}}$ giving the available free volume as $V=V^{\mathrm{system}}-V^{\mathrm{ex}}$. This volume V was used in the mean field simulation instead of the actual system volume V^{system}.

C. Results for the Compact Cluster Model

The vacancy aggregation-fragmentation model described in the preceding three sections was solved numerically by time integration using the explicit Euler method with an adaptive time stepping algorithm.[49] In all the following, the enthalpic barrier, ΔE_B, was set to zero. This assumption is based on the observation that no significant barrier beyond the activation energy for migration has been found for vacancy-vacancy reaction or vacancy-self-interstitial recombination.[45] A summary of all thermophysical properties is given in Table I.

Figure 4 shows the comparison between the atomistic data and the predictions of the continuum model with all parameters taken from Paper I and also from the previous sections in this article. A total of four components of the size distribution are used for comparison; two individual components [number of monomers (X_1) and dimers (X_2)] and two moment-based quantities [total cluster number (M_0) and average cluster size (M_2/M_1)]. The small size of the system and short simulation times preclude the quantitative use of higher-order moments. The average cluster size is defined here as the ratio of the second and first moments of the size distribution, M_2/M_1, where $M_i=\sum_s s^i X_s$ and X_s is the number of clusters of size s.

TABLE I. Thermophysical property information used in the compact cluster continuum model for vacancy cluster nucleation and growth.

Property	Value
ΔE^B	0 eV
D_1	3.37×10^{-5} cm^2/s
D_N	$9.40N^{-1.25}$ cm^2/s, $N\geqslant2$
G_N^F	$3.23N^{0.64}-T(4.34\times10^{-4}N^{0.67})$ eV
R_N^{tot}	$4.33N^{0.2}$ A

While the agreement between the atomistic data and the predictions of the continuum model is qualitatively reasonable, at least for shorter times, some of the details of the vacancy cluster evolution are not captured well by the continuum model. At longer times, the power-law evolution of the total cluster number and average size are not well captured. The continuum model in fact predicts substantially faster evolution during the later stages of the simulation. Similar conclusions are drawn for the evolution of the monomer and dimer concentrations. In the following section, an explanation for the discrepancy is given and an enhanced model is proposed. The enhanced model is then used to discuss the sensitivity of our results to the various physical components described in Secs. II and III.

V. DYNAMIC CLUSTER MODELS

In order to investigate the possible reasons for the observed discrepancy between the predictions of the continuum and atomistic model in Fig. 4, the actual cluster geometries predicted during the atomistic simulation were analyzed in detail. It is important to note that if the HRC model is accepted as an accurate representation of cluster geometries at

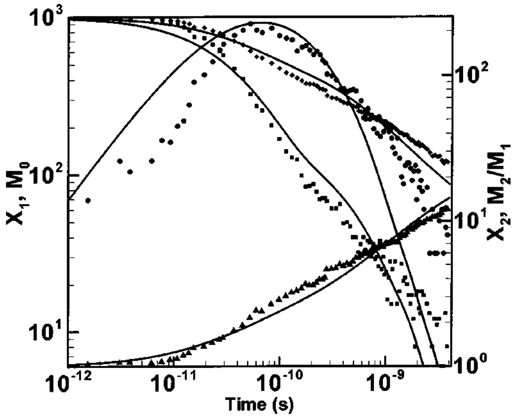

FIG. 4. Comparison between direct atomistic and compact cluster model predictions for the evolution of several components of the vacancy cluster size evolution in a closed system. Evolution profiles are for X_1 (squares), X_2 (circles), M_0 (diamonds), and M_2/M_1 (triangles).

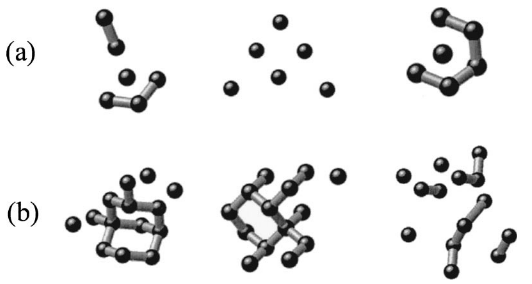

FIG. 5. Nonequilibrium cluster configurations for thermally excited clusters as observed during atomistic simulation: (a) V_6 and (b) V_{14}.

high temperature, then there are no remaining fitting parameters in the model.

Several examples of 6- and 14-vacancy clusters are shown in Fig. 5. Clearly, these species do not correspond to the predictions of the equilibrium HRC model and exhibit branches rather than fully closed rings and cages.[44] Furthermore, many of the cluster species are not completely connected by NN bonds, but rather by 2NN and even 3NN distances. In fact, one of the six-vacancy clusters is composed entirely of 2NN interactions. Similar observations can be made regarding other cluster sizes. While the HRC structure is the lowest energy configuration, cluster diffusion at high temperature necessarily implies that diffusing clusters spend a substantial fraction of time in other, higher energy, and more extended configurations. The driving force for larger clusters to assume non-HRC shapes at high temperature is likely to be a result of the importance of entropy. The latter point is analogous to the original high-temperature extended point defect picture proposed by Seeger and Chik.[50]

A. Models for Effective Cluster Size

The nonequilibrium cluster structures found during the atomistic simulation imply that both the geometrical (i.e., size) and free energy models used in the continuum model must be modified to account for thermal excitation. Cluster geometry was investigated using our previously introduced separation function:

$$r_{\mathrm{sep}}^{n}=\sqrt{\sum_{i,j>i} r_{ij}^{2}}. \tag{5.1}$$

This function represents the total of the inter-vacancy distances within a cluster. The complete set of cluster data generated by the large-scale atomistic simulation was used to determine the distribution of r_{sep}^{n} for clusters in the size range $2 \leqslant n \leqslant 16$. While larger clusters were observed during the simulation, the statistics for these sizes are poor because of the limited number of samples, and the relatively short observation times.

The distributions of r_{sep}^{n} for certain clusters are plotted in Fig. 6. Larger values of r_{sep}^{n} for a given cluster indicate more branching and a higher number of 2NN and 3NN vacancy interactions. Also shown in Fig. 6 are Maxwell-Boltzmann fits to the observed distribution of r_{sep}^{n} for each cluster. The good agreement between the data and the fits demonstrates that, for a given cluster size, configurations are distributed in equilibrium according to their energies, analogously to the distribution of (say) atomic velocities in a solid at finite temperature. This observation suggests that the configuration-sampling rate is rapid compared to the overall simulation timescale. The r_{sep}^{n} corresponding to the HRC structure for each cluster appears at the extreme left of each distribution curve (i.e., the smallest r_{sep}^{n} value) and is rarely observed.

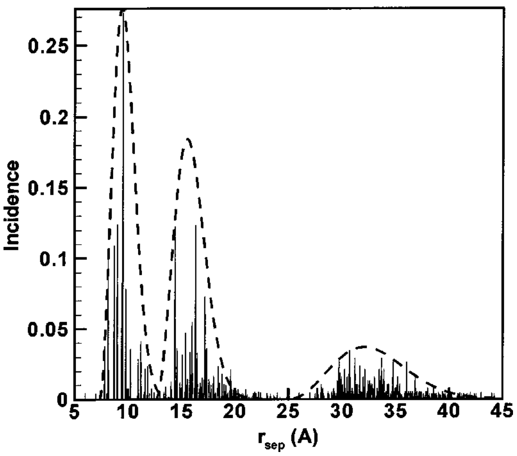

FIG. 6. Distribution of r_{sep}^{n} for clusters of sizes $n=4$, 6, and 10, calculated directly from instantaneous cluster size distribution snapshots taken throughout the entire atomistic simulation.

While the data in Fig. 6 show that clusters assume a distribution of shapes and effective sizes, it does not lead to a clear approach for determining a single effective cluster size for use in the continuum representation. The fact that the distributions appear to be near-equilibrium, indicates that each cluster samples its possible configuration states often. This notion is supported by the diffusion analysis for dimers and trimers discussed in Paper I, which showed the rapid exchange between the different configurations. Considered next are three models for effective cluster size as a function of the number of vacancies. Each of these models is subsequently tested in the continuum model.

1. Model 1—Average Sphere Model

In this model, the effective radius for a cluster of N vacancies is computed by assuming that each configuration found in the actual simulation is approximately spherical. The capture volume of each configuration is computed by tagging every atom within the 2NN interaction distance of any of the vacancies in a given cluster. In this way, the lattice strain interaction between any two clusters, 4NN-110, (see Sec. IV) is divided equally amongst the two clusters and both R_j and r_{str} in Eq. (4.1) are included in the cluster radius. This assignment of total cluster radius is valid because as shown in Sec. IV, the extent of the lattice distortion component, r_{str} is independent of cluster size. The effective volume for a cluster containing N vacancies is then given by an average over all configurations observed in the molecular dynamics simulation.

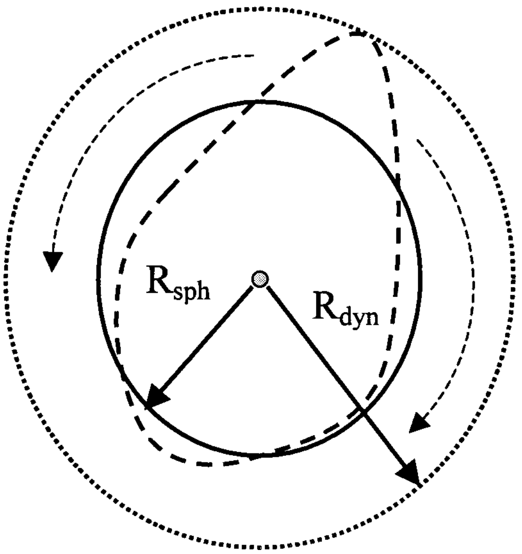

FIG. 7. Schematic representation of capture volume enhancement due to cluster shape fluctuations. R_{sph} and R_{dyn} represent different capture radii (volumes) for two configurations of the same (dynamic) cluster.

2. Model 2—Average Dynamic Cluster Model

In this model, clusters are assumed to be aspherical in shape and also to be dynamically evolving objects. Each cluster is assumed to sample its available configuration states rapidly relative to the overall aggregation timescale. The net effect is rapid cluster wobble (or equivalently, rotation) in which a spherical volume equal to the average of the maximum cluster radius of each observed configuration is incorporated into the cluster capture zone. Here, the maximum radius for each cluster configuration is computed by finding the position of the atom farthest from the cluster center-of-mass. Once again, all atoms within the 2NN interaction distance of any vacancy in the cluster are included in the total capture volume. A schematic representation of the model is shown in Fig. 7 using a single configuration as an example.

The average dynamic cluster model can be justified based on an order-of-magnitude analysis of the relevant timescales. The necessary condition for rapid configuration sampling is $t_{\mathrm{cs}} \ll t_D$, where t_{cs} is the configuration sampling time scale of a cluster containing i vacancies and $t_D = l^2/(D_i + D_j)$ is the diffusion time scale associated with the approach of a cluster of size j towards the reference cluster of size i. The length scale l can be taken as the diameter of the reference cluster, i. Configuration sampling is based primarily on the diffusion of single vacancies within the cluster, and for larger clusters, more vacancies are available for configuration changes. Thus $t_{\mathrm{cs}} \sim \delta^2/iD_1$, assuming that every vacancy hop (δ is a bond length) corresponds to a configuration change. Therefore, the "wobbling" cluster model requires that $1/D_1 \ll i^{5/3}/(D_i + D_j)$, where it was assumed that $l \sim i^{1/3}$. Clearly, this condition is met for most cases of cluster-cluster coalescence, except possibly in the case of monomer diffusion towards a small cluster, because single vacancies diffuse rapidly relative to clusters. Note that the case of monomer-monomer reaction does not need to fulfill the above requirement, because no cluster wobble is possible for monomers.

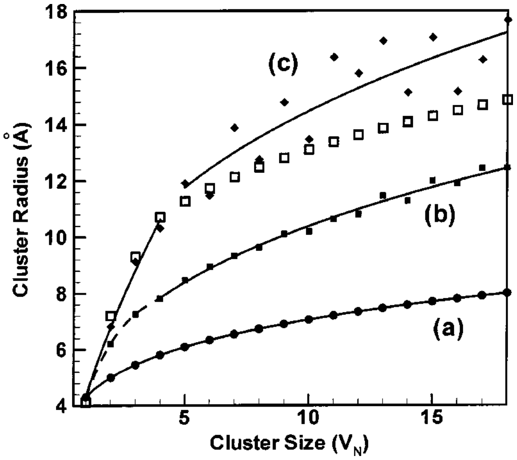

FIG. 8. Evolution of cluster radius as a function of size as predicted by the (a) average sphere model, (b) average dynamic cluster model, and (c) maximal dynamic cluster Model. Lines are power-law fits. Open squares represent an optimized capture model.

3. Model 3—Maximal Dynamic Cluster Model

The third model for cluster capture volume assumes that configuration sampling is essentially infinitely fast compared to the diffusion timescale. As a result, the maximum cluster radius (as defined in model 2) associated with the *largest* configuration appears sufficiently often to incorporate a spherical volume around the cluster. The assumption embodied in this model is more difficult to justify because it is not possible to determine how often the largest configuration is visited. While the analysis for dimer and trimer diffusion presented in Paper I demonstrated that many configurations are sampled frequently, it is quite unlikely that this effect is as pronounced for larger clusters.

Cluster radii (including the 2NN capture shell around each cluster) as a function of number of vacancies in each cluster are shown in Fig. 8 for each of the three models. Several features are worth mentioning. First, as expected, the monomer radius is equal for all three models (and corresponds to the 2NN distance) because of the spherical nature of the single vacancy capture volume. Also as expected, model 1 leads to the smallest cluster capture volumes, while model 3 predicts the largest ones. The lines shown in Fig. 8 represent power law fits of each model. The maximal dynamic cluster model shows the most scatter for larger clusters because of less statistical sampling time for these sizes.

B. Results for the Noncompact Cluster Model

The final inputs required to completely specify quantitatively any of the dynamic cluster models are free energies for each cluster size. An appropriate function for the dynamic cluster free energies is much harder to determine *a priori*, requiring knowledge of the free energy of every conformer. Instead, it is assumed that the effective free energy will continue to scale as a power law in size, as demonstrated for the equilibrium HRC structures in Refs. 22 and 44, but with slightly different parameters, which are treated here as fitting parameters. The parametric free energy model is therefore given by

$$G^{f}(n)=\alpha n^{\gamma}, \tag{5.2}$$

where α and γ are the adjustable parameters. Given that most of the configurations lead to spheroidal capture volumes, we will assume further that the free energy exponent, γ, is approximately 0.66, as would be appropriate for spheres. Based on results in Ref. 44 (i.e., $\gamma=0.63$ for HRC clusters), this value is likely to be a good representation. The pre-exponent, α, is then adjusted by optimization based on simulated annealing (SA).[49,51,52] Convergence to a global minimum is not guaranteed with most practical implementations of SA,[49] therefore all optimization results presented below were confirmed by several runs in which the initial guesses were varied.

The results obtained with each of the three models presented in Sec. V B are shown below in Fig. 9. Clearly, model 3 is able to represent the atomistic data better than models 1 or 2. Both of the latter predict substantially slower evolution that is found in the atomistic simulation. In each case, the deviation at a very early time ($t<0.05$ ns) is due to the boundary conditions imposed in the atomistic simulation, in which single vacancies were placed in a uniform grid at equal spacing. Thus, a short lag in the evolution profile is observed, followed by a slight increase in the aggregation rate once the vacancies have diffused across their initial separation distance. Note that the results shown in Figs. 9(a)–9(c) represent the best fit with respect to the parameter α. The corresponding best-fit free energy curves for each of the three models are shown in Fig. 10, along with the free energy curve predicted for HRC clusters.[44] Only a very limited number of α values lead to a reasonable fit to the atomistic data and it is not possible to use α to compensate for the different assumptions embodied in each of the three capture radius models. In other words, lowering α for model 1 would likely increase the predicted nucleation rate, but the resulting slopes would change dramatically leading to a poorer fit of the data.

The fitted value of α for model 3 leads to a free energy curve that is almost identical with the HRC free energy model, at least in the cluster size range shown (larger sizes are not relevant in the current simulation timescale). This reflects the fact that the free energy of the different conformers at each size are not very different from that of the HRC configuration at high temperature, which is consistent with the high configuration sampling rate that is observed in Fig. 6. The slightly lower free energy curves obtained with the other two models demonstrates an attempt by the optimizer to increase the aggregation rate by compensating for the underestimate in the cluster capture volumes. It is also worthwhile noting that the fitted free energy for model 3 is the only one that is higher than the HRC curve. Given that the HRC structure is known to be the lowest energy configuration,[43,44] the free energy curves fitted with models 1 and 2 can be discarded as being unphysical.

At long times (i.e., $t>3$ ns) model 3 predicts a somewhat higher nucleation rate than that observed in the atomistic simulation, as shown by the slightly steeper slopes for the average cluster size (M_2/M_1) and the total cluster number (M_0). This indicates that model 3, while the best of the three models, is a slight overestimate for the cluster capture radii. The best possible capture model was determined empirically using the SA optimization scheme, in which the cluster capture radii were allowed to fluctuate along with the free energy pre-exponent. The resulting capture radius evolution as a function of cluster size is shown in Fig. 8 (open squares). For small cluster sizes, i.e., $n<5$, the fitted capture model is essentially identical to model 3, but clearly model 3 is an overestimate for larger cluster sizes. The resulting size distribution for the optimized capture radius model is shown in

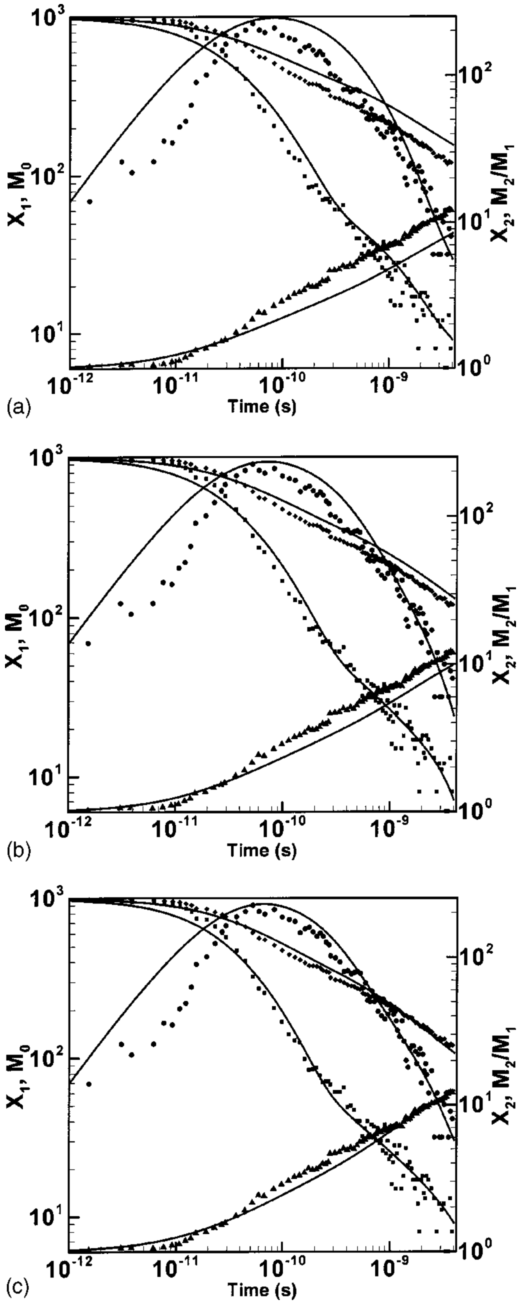

FIG. 9. Evolution profiles for each of the dynamic cluster models. (a) Model 1. (b) Model 2. (c) Model 3.

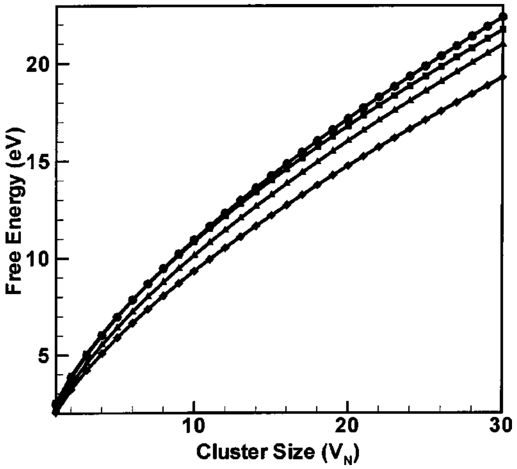

FIG. 10. Cluster free energies as a function of cluster size for: (a) the HRC model (squares), (b) model 1 (diamonds), (c) model 2 (triangles), and (d) model 3 (circles).

Fig. 11, and is very similar to the prediction of model 3 but corrects the overestimate of the aggregation rate at larger times, leading to excellent agreement between the continuum and atomistic data across the entire simulation time.

C. Discussion and analysis

The notion that vacancy clusters at high temperature exhibit center of mass diffusion and internal configurational motion has been demonstrated conclusively. Based on the discussion in Sec. V A 1 and results in Fig. 6, it is clear that configurational sampling occurs rapidly on the time scale of center of mass diffusion in all cases except for possibly monomer-cluster reaction. However, it is unlikely that the maximum-size configuration is visited sufficiently often to justify the use of model 3.

An explanation for the observed results is proposed as follows. Consider a reference cluster *i*, centered about the origin. At certain time intervals, a second cluster *j* is placed randomly (i.e. with a uniformly distributed separation) somewhere in between the surface of the most compact configuration and the surface mapped out by the largest configuration (i.e., by the size predicted by model 3). As the reference cluster, *i*, samples its different configurations, it will coalesce with cluster *j* after a time interval, $\Delta t[r_{ij},r_{\text{cap}}(i,j)]$, which is a function of the sampled sizes and the initial separation distance, r_{ij}. For small separations, the incoming cluster will be captured rapidly by any of the sampled configurations, while for larger separations only the larger configurations will lead to aggregation. In this picture, model 2 is clearly the most appropriate interpretation of the effective cluster capture volume, because the entire size distribution of cluster configurations is sampled uniformly.

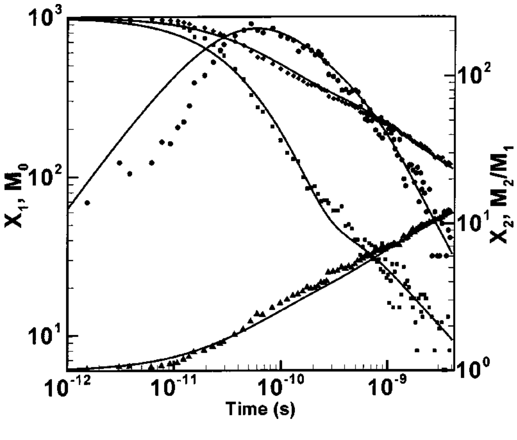

FIG. 11. Size distribution evolution for optimized capture radius model.

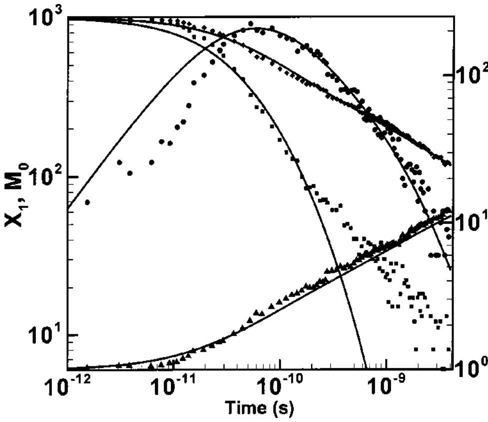

FIG. 12. Cluster size evolution in the absence of dissolution.

However, in practice this is not the case. As the incoming cluster diffuses towards the reference cluster, the tails of the distributions (right hand sides) shown in Fig. 6 are sampled first. Only if capture does not occur at this point is the rest of the distribution sampled! In fact, it is extremely unlikely that configurations smaller than the average will contribute to the effective cluster size. For rapid "internal diffusion" and configuration sampling, the largest few configurations will almost always lead to aggregation. This interpretation explains why model 3 is the best description, and why it is only a slight overestimate of the cluster capture volume.

VI. SENSITIVITY ANALYSIS

The ability of the continuum/atomistic comparison to distinguish between different mechanistic assumptions depends critically on the sensitivity of the continuum model predictions to the various model elements, i.e., reaction/dissolution model, capture radius, cluster mobility, and the free energy description. The ability of our framework to require that the correct physics be used was tested by intentionally adjusting some of the physics embodied within the model, and then attempting to maintain the agreement with respect to the atomistic data by readjusting any fitting parameters. Once again, it is worthwhile noting that the only adjustable parameter in the continuum model is the free energy prefactor—all other parameters were derived from atomistic simulations. In each of the following studies, the optimized capture radius model (Fig. 11) was used first to test the effect of different model components, *without any additional parameter fitting*.

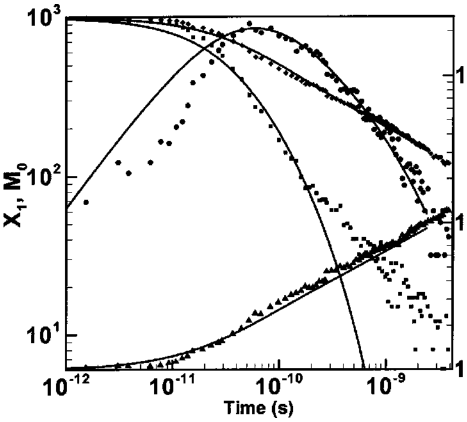

FIG. 13. Cluster size evolution in the absence of configurational entropy.

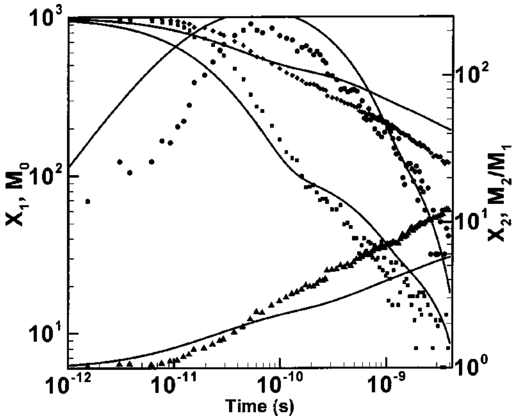

FIG. 14. Cluster size evolution in the absence of cluster mobility.

A. Cluster dissociation and entropic effects

The effect of cluster dissociation was probed first by restricting cluster dissolution. As shown in Fig. 12, the evolution profile is not affected at early times because the forward driving force is very high due to the large initial supersaturation of single vacancies, and the backward rate barrier prevents any dissolution. Furthermore, only a few clusters have formed that are available to contribute to the overall dissolution rate. However, at longer times (i.e., $t > 1$ ns) the "aggregation only" model clearly overestimates the rate of monomer consumption and the concentration of single vacancies is observed to decay to zero before the end of the simulation. Note that the moments of the overall distribution (M_0 and M_2/M_1) are not affected significantly, *highlighting the necessity for considering multiple metrics in order to test a given mean-field theory.*[27,28,53]

Similar effects are observed if dissolution is included in the usual manner but the configurational entropy term is neglected in Eq. (2.11); see Fig. 13. Once again, an overestimate of the rate of single vacancy depletion is observed. The configurational entropic effect in fact can be seen clearly in the atomistic data in the form of a kink in the single vacancy profile at about approximately 0.1 ns, which is now absent. Note that the onset of dissolution kinetics (which are driven by the configurational entropy term) is predicted correctly in the full model (Fig. 11). The depletion of single vacancies represents the largest loss of configurational entropy in the system and therefore these species are affect most severely if this mechanism is neglected. In both of the above cases, it is not possible to "compensate" for these mechanistic omissions by seeking a different value of the fitting parameter α.

B. Cluster diffusion

As discussed in Paper I, many previous efforts[1,2,3,29,31,32] aimed at predicting the distribution of vacancy (and self-interstitial) aggregates during the growth and processing of Si crystals and wafers have neglected the effect of cluster diffusion. Figure 14 demonstrates the effect on the nucleation rate if this mechanism is omitted. In particular, the overall nucleation rate is greatly underestimated and all components of the cluster evolution are affected. The reason for the dramatic difference in the predicted nucleation rate is readily explained by considering that cluster diffusion not only enhances the rate of monomer-cluster reaction, but also provides additional, parallel reaction pathways for nucleation to proceed. It is important to note that this effect might be less significant during coarsening at lower temperatures, and this issue will be addressed further in a future publication. However, it is readily apparent that an increase in the nucleation rate is likely to have some impact on any subsequent cluster growth. Specifically, the extension of the nucleation phase beyond the point at which single vacancies are exhausted should lead to larger, more stable nuclei.

C. Parametric consistency

The inclusion of dynamic cluster capture radii was not immediately obvious during the development of the final model. Using model 1 (static capture radii), a detailed parametric search analysis was performed to determine the conditions under which it was possible to reproduce the atomistic size evolution data. Figure 15 shows the predictions using model 1 if the cluster diffusion coefficients are raised by a factor of 4. Clearly, the predictions are very good, with the possible exception of the slope of the monomer curve at later

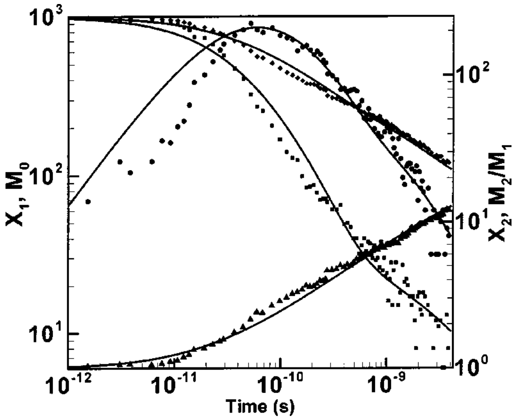

FIG. 15. Cluster size distribution predicted with the average sphere model (model 1 in Fig. 9) but with cluster diffusion increased by a factor of 4.

times. This experiment demonstrates that it is indeed possible to get good fits with other assumptions, but *not* without compromising parametric consistency. The success of this particular model variant led to several checks of the cluster diffusion calculations, but no increase could be justified, indicating that another aspect of the model was incorrect, leading to the development of models 2 and 3.

VII. CONCLUSIONS

A highly detailed analysis of vacancy cluster aggregation in Si was used to demonstrate the application of internally consistent comparisons between atomistic and continuum representations of the same process to determine systematically and quantitatively the mechanistic components required for developing accurate mean-filed models of atomic-scale events. In order to generate sufficient atomistic data to capture the size distribution evolution of clusters, a state-of-the-art parallel molecular dynamics simulation code was developed which allowed the simulation of large numbers of particles and time steps. By ensuring as far as possible parametric consistency between the atomistic and continuum approaches, it was possible to obtain a sensitive and quantitative probe into the quality of each model component. The final mean-field model demonstrates new features of vacancy cluster nucleation at high temperature that potentially will have a significant impact on crystal growth and wafer thermal annealing process simulator quality.

It was shown that the description of cluster capture volumes is difficult to estimate *a priori* and appears to be larger than would be expected based purely on static geometric analyses. This effect appears to enhance significantly the nucleation rate at the time scale investigated here, leading to fewer but bigger clusters. The effect of enhanced capture radii for larger length and time scales, where cluster coarsening is the primary process still needs to be investigated in order to determine whether this model is able to rectify some existing problems in void formation process models. Furthermore, the effect of cluster diffusion, which is often neglected in continuum process models, was shown to further increase the nucleation rate.

The sensitivity analysis in Sec. VI demonstrated clearly that every element of the continuum model described in Secs. II and III is required to produce the correct size evolution with consistent parameters. While, in principle, several variations of the mean-field description can lead to acceptable representations of the atomic data, a very tight constraint was placed on the allowable models once parametric consistency was imposed as demonstrated in Sec. VI. Many different variations of the final model were tested but none were found to reproduce the atomic data with acceptable parameters until the notion of dynamic capture radius enhancement was investigated in detail.

The overall approach demonstrated here and in Paper I is, in principle, applicable to any system and process that can be investigated directly with molecular dynamics (or the continuous Monte Carlo method). The ability to simulate atomistically larger systems for longer times will further increase the resolution to which a particular model can be unambiguously specified. As shown in this work, it is necessary to consider as many distribution components as possible when evaluating the success of a given model. Larger simulations will allow for the consideration of higher-order moments, which are even more sensitive to inaccurate assumptions.

ACKNOWLEDGMENTS

This work was supported by an NSF CAREER Award (CTS01-34418), Wacker Siltronic AG, and the ACS Petroleum Research Fund (PRF No. 36923-G5). We would also like to thank John Crocker for many fruitful discussions along the way.

---

*Corresponding author. Email address: talid@seas.upenn.edu

[1] T. Sinno, R. A. Brown, W. von Ammon, and E. Dornberger, J. Electrochem. Soc. **145**, 302 (1998).

[2] K. Nakamura, T. Saishoji, T. Kubota, T. Iida, Y. Shimanuki, T. Kotooka, and J. Tomioka, J. Cryst. Growth **180**, 61 (1997).

[3] T. Sinno and R. A. Brown, J. Electrochem. Soc. **146**, 2300 (1999).

[4] A. V. Osnipov, S. A. Kukushkin, F. Schmitt, and P. Hess, Phys. Rev. B **64**, 205421 (2001).

[5] L. Granasy and P. F. James, J. Chem. Phys. **113**, 9810 (2000).

[6] M. J. Caturla, Comput. Mater. Sci. **12**, 319 (1998).

[7] H. Zimmermann and H. Ryssel, Ann. Phys. (N.Y.) **55**, 121 (1992).

[8] H. Bracht, N. A. Stolwijk, and H. Mehrer, Phys. Rev. B **52**, 16 542 (1995).

[9] T. Frewen and T. Sinno (unpublished).

[10] M. P. Allen and D. J. Tildesley, *Computer Simulations of Liquids* (Clarendon, Oxford, 1987).

[11] D. Frenkel and B. Smit, *Understanding Molecular Simulation* (Academic, San Diego, 1996).

[12] T. Sinno, Z. K. Jiang, and R. A. Brown, Appl. Phys. Lett. **68**, 3028 (1995).

[13] P. J. Ungar, T. Halicioglu, and W. A. Tiller, Phys. Rev. B **50**, 7344 (1994).

[14] G. H. Gilmer, T. Diaz de la Rubia, D. M. Stock, and M. Jaraiz, Nucl. Instrum. Methods Phys. Res. B **102**, 247 (1995).

[15] R. Car and M. Parinello, Phys. Rev. Lett. **55**, 2471 (1985).

[16] S. K. Estreicher, Phys. Status Solidi B **217**, 513 (2000).

[17] R. Virkunnen, M. Alatalo, M. J. Puska, and R. M. Nieminen, Comput. Mater. Sci. **1**, 151 (1993).

[18] J. Zhu, T. Diaz de la Rubia, L. H. Yang, and C. Mailhiot, Phys. Rev. B **54**, 4741 (1996).

[19] T. Sinno, *Thermophysical Properties of Intrinsic Point Defects in Crystalline Silicon* (The Electrochemical of the Society, Pannington, NJ, 2002).

[20] A. La Magna and S. Coffa, Comput. Mater. Sci. **17**, 21 (2000).

[21] M. Jaraiz, L. Pelaz, E. Rubio, J. Barbolla, G. H. Gilmer, D. J. Eaglesham, H.-J. Gossmann, and J. M. Poate, in *Silicon Front-End Technology—Materials Processing and Modeling*, edited by N. E. B. Cowern, D. C. Jacobson, P. B. Griffin, P. A. Packan, and R. P. Webb, MRS Symposia Proceedings No. 532 (Materials Research Society, Warrendale, PA, 1998), p. 43.

[22] M. Prasad and T. Sinno (unpublished).

[23] M. Itsumi, H. Akiya, T. Ueki, M. Tomita, and M. Yamawaki, J. Appl. Phys. **78**, 5984 (1995).

[24] E. Dornberger, D. Temmler, and W. von Ammon, J. Electrochem. Soc. **149**, G226 (2002).
[25] M. Z. Bazant, E. Kaxiras, and J. F. Justo, Phys. Rev. B **56**, 8542 (1997).
[26] J. F. Justo, M. Z. Bazant, E. Kaxiras, V. V. Bulatov, and S. Yip, Phys. Rev. B **58**, 2539 (1998).
[27] C. M. Sorensen, H. X. Zhang, and T. W. Taylor, Phys. Rev. Lett. **59**, 363 (1987).
[28] F. Family, P. Meakin, and J. M. Deutch, Phys. Rev. Lett. **57**, 727 (1986); **52**, 2332(E) (1986).
[29] R. Habu and A. Tomiura, Jpn. J. Appl. Phys. **35**, 1 (1996).
[30] M. V. Smoluchowski, Z. Phys. Chem. **92**, 192 (1917).
[31] E. Dornberger, J. Esfandyari, D. Graf, J. Vanhellemont, U. Lambert, F. Dupret, and W. von Ammon, in *Crystalling Defects and Contamination: Their Impact and Control in Device Manufacturing II*, edited by B. O. Kolbesen, P. Stallhofer, C. Claeys, and F. Tardiff (The Electrochemical Society, Pennington, NJ, 1997), PV 97-22, p. 40.
[32] M. Schrems, P. Pongratz, M. Budil, H. W. Potzl, J. Hage, E. Guerrero, and D. Huber, presented at the Proceedings of the Sixth International Symposium on Silicon Materials Science and Technology: Semiconductor Silicon, 1990.
[33] D. Kashchiev, *Nucleation: Basic Theory with Applications* (Oxford University Press, Boston, 2000).
[34] L. A. Girifalco, *Statistical Mechanics of Solids* (Oxford University Press, New York, 2000).
[35] J. L. Katz and H. Weidersich, J. Chem. Phys. **55**, 1414 (1971).
[36] D. Turnbull and J. C. Fisher, J. Chem. Phys. **17**, 71 (1949).
[37] T. R. Waite, J. Chem. Phys. **28**, 103 (1958).
[38] I. M. Lifshitz and V. V. Slyozov, J. Phys. Chem. Solids **19**, 35 (1959).
[39] F. C. Collins and G. E. Kimball, J. Colloid Sci. **4**, 425 (1949).
[40] F. S. Ham, J. Appl. Phys. **30**, 1518 (1959).
[41] J. Frenkel, *Kinetic Theory of Liquids* (Dover, New York, 1955).
[42] M. Volmer, *Kinetik der Phasenbildung* (Steinkopff, Dresden, 1939).
[43] A. Bongiorno, L. Colombo, F. Cargnoni, C. Gatti, and M. Rosati, Europhys. Lett. **50**, 608 (2000).
[44] M. Prasad and T. Sinno, Appl. Phys. Lett. **80**, 1951 (2002).
[45] A. Bongiorno and L. Colombo, Phys. Rev. B **57**, 8767 (1998).
[46] J. A. Van Vechten, Phys. Rev. B **33**, 2674 (1986).
[47] M. Itsumi, H. Akiya, T. Ueki, M. Tomita, and M. Yamawaki, J. Appl. Phys. **78**, 5894 (1995).
[48] M. Itsumi, J. Cryst. Growth **210**, 1 (2000).
[49] W. H. Press, S. A. Teukolsky, W. T. Vetterling, and B. P. Flannery, *Numerical Recipes in Fortran* (Cambridge University Press, Cambridge, 1992).
[50] A. Seeger and K. P. Chik, Phys. Status Solidi **29**, 455 (1968).
[51] J. A. Nelder and R. Mead, Comput. J. (UK) **7**, 308 (1965).
[52] L. Ingber, Math. Comput. Model. **15**, 77 (1991).
[53] S. Chakravarthi and S. T. Dunham, J. Appl. Phys. **89**, 4758 (2001).